Check for updates

Low temperature hydrodeoxygenation of guaiacol into cyclohexane over Ni/SiO$_2$ catalyst combined with Hβ zeolite

Xun Wang,[a] Shanhui Zhu, [iD] *[b] Sen Wang, [iD] [b] Yue He,[b] Yang Liu,[bc] Jianguo Wang, [iD] [b] Weibin Fan [iD] [b] and Yongkang Lv*[a]

Hydrodeoxygenation (HDO) of guaiacol to cyclohexane, important for bio-oil upgrading, is usually performed at high reaction temperature (≥200 °C). In this work, low temperature transformation of guaiacol to cyclohexane was achieved at 140 °C over non-noble metal Ni/SiO$_2$ and various zeolites. Among zeolites tested (HUSY, HMOR, Hβ, HZSM-5, SAPO-34), Hβ zeolite exhibited superior catalytic activity due to its appropriate pore structure and acid strength. The open pore with three-dimensional structure of Hβ facilitates the diffusion of guaiacol and intermediates. Meanwhile, weak acid strength of Hβ efficiently reduces the competitive adsorption of guaiacol, and then promotes the dehydration of intermediate 2-methoxycyclohexanol. Moreover, the catalytic performance in guaiacol HDO to cyclohexane is also closely related to Si/Al ratio of Hβ. Owing to its moderate acid density, the maximum yield of cyclohexane reaches 91.7% on Hβ(Si/Al = 50) combined with Ni/SiO$_2$ at 140 °C, which is the lowest temperature ever reported over non-noble metal catalysts.
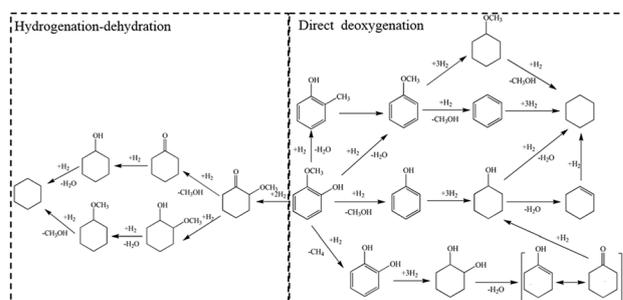
1. Introduction

Bio-oil, produced by liquefaction or fast pyrolysis of biomass, is a promising liquid fuel and chemical raw material in light of the decreasing fossil fuels and increasing air pollution.[1–3] However, bio-oil cannot be directly used as transportation fuel without any treatment due to its high oxygen content, which leads to high viscosity, chemical and thermal instability of fuels.[4] Hydrodeoxygenation (HDO) is deemed as the most effective method for bio-oil upgrading, which can reserve the calorific value profitably.[4–7] Owing to the complex composition of bio-oil, HDO of bio-oil's model compounds raises wide concern to research on the mechanism of bio-oil upgrading. Guaiacol, at good yield in bio-oil, contains two types of C–O bonds, sp^2 C$_{aryl}$–O and sp^3 CH$_3$–O, which are prevalent in bio-oil. Due to its high calorific value, catalytic HDO of guaiacol into cyclohexane, a kind of fully deoxygenated product, is an excellent model reaction for bio-oil upgrading.

Currently, a variety of catalysts have been developed for the transformation of guaiacol to cyclohexane. In 2009, Kou[6] firstly reported a new catalytic route with a bifunctional combination of Pd/C with H$_3$PO$_4$ for converting phenolic bio-oil components

to cycloalkanes with high selectivity. The HDO of phenolic monomers into alkanes involved metal-catalyzed hydrogenation and acid-catalyzed hydrolysis and dehydration. However, liquid acid catalyst is very corrosive. Later, various noble-metals supported on solid acid carriers were employed for the HDO of guaiacol to cyclohexane. The group of Ha[8] got cyclohexane at good yield of 60% at 250 °C over Ru/SiO$_2$–Al$_2$O$_3$. In addition, Pt supported on various zeolites[9] exhibited HDO performance of guaiacol to different degrees. Pt/Hβ got the highest yield (about 45%) of cyclohexane at 250 °C. Grunwaldt *et al.*[10] achieved 93% yield of cyclohexane from guaiacol over Pt/H-MFI-90 at moderate temperature of 180 °C. Scheme 1 provides an overview on the reaction pathways of guaiacol HDO in the presence of noble-metal catalysts. One pathway is deoxygenation as a first step, and the other way is hydrogenation of aromatic ring

[a] Key Laboratory of Coal Science and Technology, Ministry of Education and Shanxi Province, Taiyuan University of Technology, Taiyuan 030024, Shanxi, China. E-mail: lykang@tyut.edu.cn

[b] State Key Laboratory of Coal Conversion, Institute of Coal Chemistry, Chinese Academy of Sciences, Taiyuan 030001, PR China. E-mail: zhushanhui@sxicc.ac.cn

[c] University of Chinese Academy of Sciences, Beijing 100049, PR China

Scheme 1 Reaction pathway for the conversion of guaiacol over different catalysts.[10,14]

followed by acid-catalyzed dehydration. Due to the high hydrogenation activity of noble-metals, hydrogenation of aromatic ring to 2-methoxycyclohexanol (MCH) is preferred under mild condition. The selectivity towards various possible deoxygenation products (cyclohexanol, methoxycyclohexane, cyclohexane, *etc.*) are closely related to the acidity of support materials. However, high price of noble-metals will greatly limit their further applications in industry.

Considering the industrial application, base metallic catalysts with earth-abundant elements are potential candidates. Nickel-based catalysts, if designed elaborately, are promising for their high intrinsic ability of hydrogenation activity in the HDO of guaiacol. Ma *et al.*[11,12] reported that $Ni/SiO_2–ZrO_2$ effectively converted guaiacol to cyclohexane at excellent yield of 96.8% at 300 °C. Over carbon nanotubes supported Ni–Fe catalysts, Yuan and coworkers[13] gained 83.4% yield of cyclohexane at 400 °C. M. V. Bykova[14] studied the Ni-based sol–gel catalysts for guaiacol HDO and got 63.9% yield of cyclohexane at 320 °C. Over Ni-based catalysts, guaiacol HDO is mainly proceeded in two pathways as similar as noble-metal catalysts (Scheme 1), including hydrogenation of aromatic ring and direct hydrogenolysis of C–O bond, respectively. Under low temperature, hydrogenation of aromatic ring is the main reaction pathway, and Ni-based catalysts present low activity of hydrogenation. High reaction temperature can promote the activity of Ni-based catalysts on which guaiacol HDO mainly proceeds in direct hydrogenolysis pathway. However, the intermediate products of phenolic compounds in direct hydrogenolysis pathway tend to cause significant coke formation and catalyst deactivation at high temperature. Considering the complex constituents of bio-oil, it would be highly desirable to operate HDO of guaiacol under low temperature. There are two approaches to decrease the reaction temperature for guaiacol transformation to cyclohexane, namely, to enhance the intrinsic activity of catalyst or to develop a novel pathway.

Herein, we report a new bifunctional catalyst of Ni/SiO_2 physically mixed with zeolite to convert guaiacol to cyclohexane at low temperature. In our recent work,[15] a confined nano Ni/SiO_2 catalyst prepared by ammonia evaporation hydrothermal (AEH) method has been obtained, in which high-dispersed Ni nanoparticles were entrapped in fibrous nickel phyllosilicate (Fig. 1).

Owing to its unique structure, Ni/SiO_2 gave complete conversion of guaiacol and 95.5% yield of MCH at 140 °C. Similar to deoxygenation of polyols to liquid hydrocarbons,[16–18]
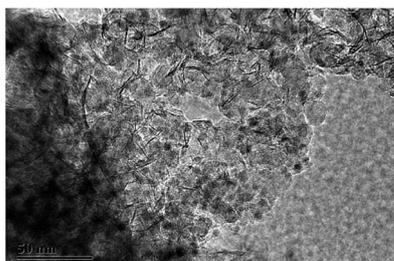

Fig. 1 TEM image of reduced Ni/SiO_2 prepared by ammonia evaporation hydrothermal method.

MCH could be further converted into alkane by acid-catalyzed deoxygenation, followed by successive hydrogenation. Compared with other solid acid catalysts, such as ion-exchanged resin, oxides and supported heteropolyacids, zeolites would be prospective choice due to their outstanding thermal stability and tunable pore properties. Therefore, various kinds of zeolites combined with Ni/SiO_2 were utilized to perform HDO of guaiacol to cyclohexane at very low reaction temperature. In this contribution, the effects of porous structure and acidic properties of zeolites were also explored on catalytic performance.

2. Experimental

2.1. Materials

The following materials were provided by various suppliers: guaiacol (Sinopharm Chemical Reagent Co., Ltd., China), decalin (Tokyo Chemical Industry). Hβ with different Si/Al ratios and HUSY were purchased from Catalyst Factory of Nankai University (Tianjin, China). Hβ with a Si/Al ratio of X was denoted as Hβ(X). These purchased zeolites were calcined at 560 °C for 4 h prior to use.

2.2. Catalyst preparation

Ni/SiO_2 was synthesized by AEH method according to our previous work.[15] ZSM-5 (Si/Al = 30), SAPO-34, and mordenite (Si/Al = 10) were synthesized by a hydrothermal method.[19,20] In a typical synthesis of ZSM-5, adequate amounts of sodium aluminate ($NaAlO_2$), tetrapropylammonium hydroxide (TPAOH), sodium hydroxide (NaOH), silica sol (JN-40) and water (H_2O) were mixed in a plastic vessel and then aged for 4 h under vigorous stirring at room temperature. The molar composition of the reactants in the solution was $1SiO_2 : 0.0167Al_2O_3 : 0.15TPAOH : 30H_2O$. Crystallization of zeolite was carried out in a Teflon-lined stainless steel autoclave at 170 °C for 48 h. The synthesized solid product was centrifuged and washed with water for several times. Then the solid product was dried at 100 °C overnight and calcined at 550 °C for 6 h. Finally, the obtained Na-form zeolite was changed into H-form by ion-exchange with NH_4NO_3 solution at 80 °C for 5 h, and then calcined at 560 °C for 6 h.

2.3. Catalytic test

Prior to the reaction, Ni/SiO_2 was prereduced at 600 °C for 2 h in flow of 10 v% H_2/Ar gas (60 mL min^{-1}). The catalytic performance of Ni/SiO_2 with different zeolites in the conversion of guaiacol was tested in a 50 mL stainless steel autoclave lined with Teflon. Typically, 0.10 g guaiacol, 20 mL decalin, 50 mg Ni/SiO_2 and a certain amount of zeolite were loaded into the autoclave. Then, the autoclave was filled with 3.0 MPa hydrogen. The reaction mixture maintained at 140 °C for a certain time.

The components of liquid products were identified by GC-MS (6890N, Agilent, USA). Quantitative analysis of the liquid products was measured with ethyl benzoate as an internal standard by gas chromatography (GC-2014C, SHIMADZU)

equipped with a flame ionization detector (FID) and a DB-WAX capillary column. Carbon balance was checked in the range of 95–99%. The conversion of guaiacol and product yield were calculated according to the following equations:

$$\mathrm{conversion}(\%)$$
$$= \frac{\mathrm{moles\ of\ guaiacol\ (initial)} - \mathrm{moles\ of\ guaiacol(final)}}{\mathrm{moles\ of\ guaiacol(initial)}}$$

$$\mathrm{yield}(\%) = \frac{\mathrm{moles\ of\ product\ }i}{\mathrm{moles\ of\ guaiacol(initial)}}$$

2.4. Catalyst characterization

The X-ray diffraction (XRD) patterns of different zeolites were performed on Rigaku MiniFlex II desktop X-ray diffractometer with Cu Kα radiation. The scanning speed was set as $4° \mathrm{min}^{-1}$.

The actual Si/Al ratio of zeolite was measured by ICP optical emission spectroscopy (Optima 2100DV, PerkinElmer).

N_2 adsorption–desorption isotherms was performed on Micromeritics TriStar 3000 instrument. Before measurement, 0.10 g sample was degassed under vacuum at 300 °C for 8 h.

The different types of acid sites in zeolite were determined by pyridine adsorption of Fourier transform infrared spectra (Py-IR) on a Bruker Tensor 27 FT-IR spectrometer. Zeolite sample was firstly pressed into self-supported wafer. Prior to measurement, the wafer was pretreated in vacuum at 350 °C for 2 h. The IR spectrum was recorded at 150 °C as reference. When the temperature fell to 35 °C, the sample was exposed to pyridine vapor for 30 min. The Py-IR spectrum was then recorded at 150 °C after vacuumizing for 60 min. The concentration of acidic sites was calculated by the procedures reported by Madeira et al.[21]

Temperature-programmed desorption of ammonia (NH_3-TPD) was performed in an Auto Chem II 2920 chemisorption analyzer. Typically, 0.10 g sample was pretreated at 550 °C for 2 h in flowing Ar (30 mL min^{-1}). Once the temperature cooled down to 50 °C, NH_3 was introduced into the system for 30 min. Subsequently, physisorbed NH_3 was removed at 120 °C for 2 h under flowing Ar. Then the sample was heated to 600 °C at a rate of 10 °C min^{-1} and the desorbed NH_3 was recorded by TCD.

2.5. Density functional theory (DFT) calculation of molecular kinetic diameters

DFT calculation was performed on Gaussian 09.D01 package. Molecule geometries were optimized by using the ωB97X-D hybrid functional and the 6-311+G(2df, 2p) basis set. Molecular kinetic diameters (d_σ) were defined as the internuclear distance (d_i) between the two nuclei that intersected the surface of the smallest possible cylinder plus an estimate of the van der Waals radii of the hydrogen (1.200 Å) or oxygen (1.520 Å) atoms involved, according to the Lennard-Jones model ($d_\sigma = d_i/21/6$), as reported by Huber,[22] Ding,[23] Gao[24] and co-workers.

2.6. FTIR study of guaiacol adsorption on zeolite

FTIR study of guaiacol adsorption on zeolite was performed on a Bruker TENSOR 27 FT-IR spectrometer. Firstly, the powder of zeolite was pressed into a self-supporting wafer, and then was placed into the IR cell. Prior to measurement, the sample was pretreated at 350 °C for 2 h in vacuum. Subsequently, guaiacol was introduced by dropping 20 μL guaiacol on the wafer. In order to remove excessive guaiacol, the cell was evacuated at 350 °C until the spectra became constant. Finally, the IR spectrum of surface species was recorded.

3. Results and discussion

3.1. Catalyst characterization

In this work, a series of zeolites combined with Ni/SiO$_2$ were used as bifunctional catalysts for one-pot HDO of guaiacol to cyclohexane through multistep reactions consisting of hydrogenation and dehydration. Thus, a crucial factor that affects this reaction rate is the diffusion of hydrogenation reaction product to the acid sites of zeolite,[25] which is closely related to the porous structure of zeolite. According to previous work,[26] the pore diameters of zeolites decline as HUSY > HMOR > Hβ > HZSM-5 > SAPO-34 (Table 1). As shown in Table 1, the pore diameters of HUSY, HMOR and Hβ zeolites are 7.4 Å, 7.0 Å and 6.7 Å, respectively, which are larger than the kinetic diameters of guaiacol (6.68 Å)[27] and MCH (6.55 × 6.67 Å) calculated by

Table 1 Physicochemical properties of zeolites

| Zeolites	Pore diameter (Å)	Channel structure	S_{BET} (m^2 g^{-1})	$V_{\mathrm{p,t}}$ (cm^3 g^{-1})	Acid sites (mmol g^{-1}) BAS	LAS	Si/Al ratio
SAPO-34	3.8 × 3.8	3D, 8-ring	562	0.31	0	0	0.1
HZSM-5	5.3 × 5.6	3D, 10-ring	375	0.34	0.35	0.08	26.3
Hβ(12.5)	6.6 × 6.7	3D, 12-ring	528	0.39	0.35	0.31	10.8
HMOR	6.5 × 7.0	1D, 12-ring	452	0.25	0.13	0.02	9.5
	5.7 × 2.6	1D, 8-ring					
HUSY	7.4 × 7.4	3D, 12-ring	516	0.29	0.92	0.28	3.3
Hβ(20)	6.6 × 6.7	3D, 12-ring	545	0.52	0.23	0.25	16.0
Hβ(50)	6.6 × 6.7	3D, 12-ring	495	0.30	0.21	0.12	49.0
Hβ(250)	6.6 × 6.7	3D, 12-ring	577	0.34	0.04	0.01	229.6
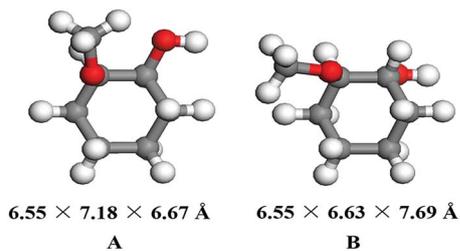
Fig. 2 Space-filling model of (A) *cis*-2-methoxycyclohexanol and (B) *trans*-2-methoxycyclohexanol.
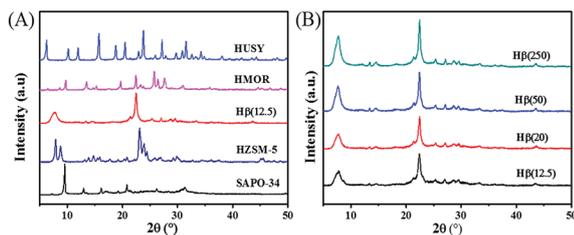

Fig. 3 XRD patterns of (A) zeolites with different structures (B) Hβ with different Si/Al ratios.

DFT theory (Fig. 2). In contrast, HZSM-5 and SAPO-34 have smaller average pore sizes (namely, 5.6 Å and 3.8 Å) than the kinetic diameters of guaiacol and MCH.

The physicochemical properties of zeolites were characterized by BET, XRD, Py-IR and NH$_3$-TPD. As shown in Table 1, all of zeolites have high surface area and pore volume. Among them, the BET surface area of SAPO-34 is the highest (562 m^2 g^{-1}), while Hβ(20) displays the maximum pore volume. The XRD patterns in Fig. 3 illustrate that all the as-synthesized zeolites are well crystallized with the characteristic peaks according to JADE 5.0. For Hβ, the crystallinity of zeolite becomes strong with an increase of Si/Al ratio.

The Py-IR profiles and acid amounts of zeolites are depicted in Fig. 4 and Table 1, respectively. As displayed in Fig. 4A, two pyridine adsorption peaks are centered at 1450 cm^{-1} and 1540 cm^{-1}, corresponding to Lewis acid sites (LAS) and Bronsted acid sites (BAS), respectively.[28,29] The peak area represents the density of acid sites. Obviously, the acid density of HUSY is highest among tested zeolites. However, no peak of pyridine adsorption was detected on SAPO-34 owing to its smaller pore size than molecular diameter of pyridine. The acidity of Hβ
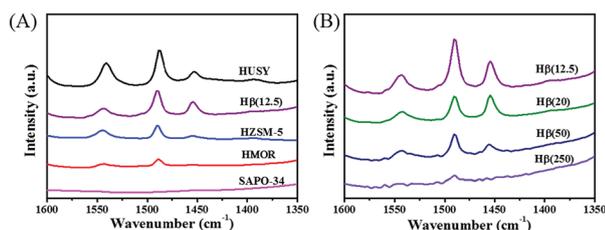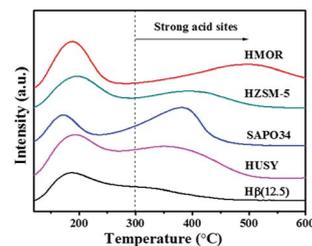

Fig. 5 NH$_3$-TPD profiles of various zeolites.

zeolite with different Si/Al ratios was also measured by Py-IR. With an increase in the Si/Al molar ratio, the amounts of BAS and LAS decrease evidently (Fig. 4B). According to quantitative analysis, the ratio of BAS to LAS increases from 0.9 to 4.0 with an increase of Si/Al molar ratio from 12.5 to 250, indicating that BAS turns into primary acid species on Hβ zeolite with high Si/Al molar ratio.[30] According to NH$_3$-TPD profiles (Fig. 5), all zeolites present two ammonia desorption peaks, one in low-temperature region and the other in high-temperature region, corresponding to weak acid sites and strong acid sites, respectively. Of the examined catalysts, HMOR has the strongest acid sites, in which the high-temperature peak is centered at 500 °C in NH$_3$-TPD profile. Hβ(12.5) has large number of weak acid sites and small amount of medium-strong acid sites, and its acid strength is lower than that of other zeolites.

3.2. FTIR study of guaiacol adsorption on zeolite

The adsorption states of guaiacol over HUSY, HMOR and Hβ were investigated by FT-IR (Fig. 6). As reference, FTIR spectrum of pure guaiacol was also measured, and the assignments of characteristic vibration peaks are listed in Table 2. After introduction guaiacol to zeolite, the positions of guaiacol characteristic peaks shift compared with that of pure guaiacol, indicating that guaiacol virtually chemisorbs on zeolite. Especially, the γ(C=C$_{ring}$) peak of pure guaiacol at 1502 cm^{-1} shifts to low wavenumber, suggesting the presence of electrodonation effect of zeolite's LAS on the aromatic ring of guaiacol.[31] However, the adsorption strength of guaiacol on various zeolites is significantly different, which can be reflected by the degree of red shift about γ(C=C$_{ring}$) vibration peak (Fig. 6A). Notably, the characteristic peak of γ(C=C$_{ring}$) shifts down to 1487 cm^{-1} and 1490 cm^{-1} after guaiacol adsorption on HMOR and HUSY, respectively. This indicates the strong interaction between

Fig. 4 FTIR profile of pyridine adsorbed on (A) zeolites with different pore structures and (B) Hβ with different Si/Al ratios.
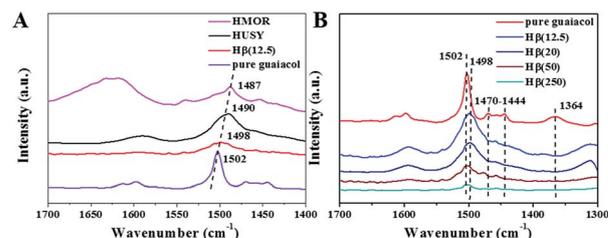

Fig. 6 IR spectra of guaiacol adsorption at 350 °C on (A) zeolites with different structures and (B) Hβ with different Si/Al ratios.

Table 2 IR characteristic peaks of pure guaiacol and their assignments[a]

Assignment	Guaiacol
$\gamma(C=C_{ring})$	1616, 1597, 1502
$\delta(CH_3)$	1444–1470
$\delta(OH)$	1364
$\gamma(C–OH)$	1260
$\gamma(C–OCH_3)$	1225

[a] The assignment is based on our experiment about IR spectrum of pure guaiacol on KBr.[15]

guaiacol and strong acid sites of zeolites, which were verified by NH_3-TPD (Fig. 5). Compared with HMOR and HUSY, the $\gamma(C=C_{ring})$ peak of guaiacol shifts downward to 1498 cm^{-1} after adsorption on Hβ, implying the relatively weak interaction between guaiacol and Hβ. Fig. 6B shows the adsorption states of guaiacol on Hβ with various Si/Al ratios. Obviously, the adsorption strength of guaiacol has less relationship to the Si/Al ratio of zeolite. However, the adsorption capacity of guaiacol on Hβ gradually reduces with increasing of Si/Al ratio owing to decreasing acid density (Table 1).

3.3. Effect of zeolite structure on guaiacol HDO

According to previous works,[6,32,33] HDO conversion of guaiacol into cyclohexane in HYD pathway contains multistep reactions consisting of metal-catalyzed hydrogenation and acid-catalyzed dehydration. In our recent work,[15] low-temperature transformation of guaiacol to MCH has been achieved in high yield (95.5%) over Ni/SiO$_2$. MCH could be converted into cyclohexane by dehydration–hydrogenation over zeolite mixed with Ni/SiO$_2$. Thus, the reaction rate of dehydration could be affected by various parameters of zeolite including pore structure, acidity, as well as the diffusion rates of reactant and product inside the zeolite pores. To gain insight into the effect of zeolite's pore structure on the product distribution, a series of typical zeolites were deliberately chosen as solid acid catalysts to explore their catalytic performance in HDO of guaiacol.

According to previous results, BAS is significantly more active than LAS for alcohols dehydration.[34] To eliminate the effect of acid density, the catalytic performance of zeolites with different channels was compared under the same content of BAS, as shown in Table 3. It is evident that the catalytic performance of Ni/SiO$_2$ mixed with zeolite strongly depends on the structure of zeolite. Among them, Hβ(12.5) exhibited uniquely active and excellent yield of cyclohexane (55.6%) with >99% conversion of guaiacol, followed by an intermediate production level of cyclohexane on HMOR (16.8%) and H-ZSM5 (50.5%). SAPO-34 and HUSY showed much lower yield of cyclohexane (0.6% and 1.6%, respectively), in contrast to other zeolites.

Compared with the maximum pore size of zeolite (Table 1) and kinetic diameter of MCH, it can be seen that MCH molecular is too large to enter the internal porous structure of SAPO-34 and HZSM-5, and then can not access the acid sites within zeolite pores. The dehydration of MCH mainly proceeds on the external acid sites, which only constitutes a very small

percentage of the total acid sites.[35] In particular, no consecutive conversion of MCH into cyclohexane occurs on SAPO-34, because it possesses no acid sites on the external surface of zeolite. For zeolites that have large pore size with 12-membered rings (i.e., Hβ, HMOR and HUSY), guaiacol and reaction intermediates can diffuse into the internal porous structure of zeolites. The dehydration of MCH can proceed not only on the external acid sites, but also in the internal porous structure of zeolites, in which acid sites account for the majority of the total acid sites.[35]

However, though HUSY and HMOR possess large pore size, low yields of cyclohexane were obtained (Table 3, entry 5 and 6). On the one hand, the poor catalytic performance may be assigned to the inherent pore structure of zeolites. HUSY is a three-dimensional channel structure containing supercage, and HMOR is a one-dimensional pore structure containing 8-ring channel. This makes it difficult for the diffusion of reactant and product,[18] resulting in lower yield of cyclohexane than that over Hβ with three-dimensional porous structure without excess space (supercage) (Table 3, entry 4). On the other hand, the low yields of cyclohexane on HUSY and HMOR are closely related to their strong acid strength. As can be seen from Fig. 6A, the adsorption strength of guaiacol on HUSY and HMOR is higher than that of Hβ due to their strong acid sites. Thus, guaiacol strongly adsorbed on the acid sites of HUSY and HMOR plugs the pore of zeolite, and then reduces the available acid sites for MCH dehydration.

Among zeolites with large size pore, Hβ(12.5) exhibited the highest reaction rate in the dehydration of MCH. Firstly, the excellent performance may be ascribed to its proper pore size and three-dimensional porous structure with no excess space (supercage). The open three-dimensional pore structure is favorable for the rapid diffusion of MCH to the internal acid sites of Hβ(12.5), leading to high reaction rate. Meanwhile, the super catalytic performance is partially assigned to its weak acid strength. As shown in Fig. 6A, the adsorption strength of guaiacol on Hβ(12.5) is lowest among zeolites with large pore size. Guaiacol could keep self balance of adsorption–desorption in pore of zeolite, which can not block the channel of zeolite. MCH can effectively diffuse to the acid sites in the hole of zeolite for dehydration. Thus, in comparison with other zeolites investigated, Hβ is the optimum one for guaiacol HDO due to its suitable acid strength and pore structure with three-dimensional (3D) system.

3.4. Effect of Si/Al ratio on guaiacol HDO over zeolite

MCH, produced from guaiacol hydrogenation on Ni/SiO$_2$, is a kind of alcohol, which could be transformed into alkane over bifunctional catalyst. That is coupling dehydration on acid sites of zeolite and hydrogenation on metal active sites. The dehydration of alcohol mainly proceeds via parallel reaction mechanism: intramolecular dehydration to alkene on BAS and intermolecular dehydration to ether depending on BAS and LAS.[36,37] Hence, the product distribution of guaiacol HDO is related to the properties of acid sites (acid density and acid type) in zeolite, affected by Si/Al ratio over zeolite.

Table 3 Hydrodeoxygenation of guaiacol over different catalysts[a]

Entry	Catalyst	Zeolite dosage (mg)	BAS (μmol)	LAS (μmol)	Conv. (%)	Yield (%)		
						Cyclohexane	Cyclohexanol	MCH[b]
1	Ni/SiO$_2$	0	—	—	>99	0.2	4.0	95.5
2	Ni/SiO$_2$ + SAPO-34	50	0	0	98.2	0.2	4.8	87.3
3	Ni/SiO$_2$ + HZSM-5	50	17.5	4.0	98.9	50.5	0.4	40.7
4	Ni/SiO$_2$ + Hβ(12.5)	50	17.5	15.5	>99	55.6	0.8	29.7
5	Ni/SiO$_2$ + HMOR	134.6	17.5	2.7	93.8	16.8	8.9	67.4
6	Ni/SiO$_2$ + HUSY	19.0	17.5	5.3	95.1	1.6	3.6	88.0

[a] Reaction conditions: guaiacol (100 mg), zeolite, Ni/SiO$_2$ (50 mg), decalin (20 mL), 3 MPa H$_2$, 140 °C, 5 h. [b] MCH: 2-methoxycyclohexanol.

Table 4 Hydrodeoxygenation of guaiacol over Ni/SiO$_2$ combined with Hβ zeolite at different Si/Al ratio[a]

| Entry	Catalyst	Acid sites (μmol)			Conv. (%)	Yield (%)	
		Total	BAS	LAS		MCH[b]	Cyclohexane
1	Ni/SiO$_2$ + Hβ(12.5)	33.0	17.5	15.5	72.0	41.1	15.6
2	Ni/SiO$_2$ + Hβ(20)	25.0	12.0	13.0	77.6	31.8	29.2
3	Ni/SiO$_2$ + Hβ(50)	15.0	9.5	5.5	97.4	5.4	79.6
4	Ni/SiO$_2$ + Hβ(250)	2.3	1.8	0.5	99.4	82.6	8.5

[a] Reaction conditions: guaiacol (0.10 g), Ni/SiO$_2$ (50 mg), Hβ (50 mg), decalin (20 mL), 140 °C, 3 MPa H$_2$, 2 h. [b] MCH: 2-methoxycyclohexanol.

Table 4 shows the catalytic performance of Ni/SiO$_2$ combined with Hβ zeolite (different Si/Al ratio) on guaiacol HDO. Obviously, Si/Al ratio of Hβ has a significant effect on guaiacol conversion and yield of cyclohexane. In the case of Hβ(12.5) (Table 4, entry 1), guaiacol conversion and cyclohexane yield were 72.0% and 15.6%, respectively. The yield of cyclohexane reached its maximum at Si/Al = 50, being 79.6%. Further increasing of Si/Al ratio to 250 declined the yield of cyclohexane. An excessively low or high Si/Al ratio is unsuitable for the production of cyclohexane.

As shown in Scheme 2, guaiacol is first converted into MCH on Ni/SiO$_2$ and then deoxygenated on acid sites of Hβ zeolite. In cascade reaction, the consecutive transformation of MCH on acid sites of zeolite should be benefit for accelerating guaiacol conversion. However, there is no positive correlation between guaiacol conversion and the concentration of acid sites over Hβ with different Si/Al ratios. Despite possessing highest acid density, Hβ(12.5) exhibited low conversion of guaiacol and

Scheme 2 Proposed reaction pathway for guaiacol conversion over Ni/SiO$_2$ combined with Hβ.

cyclohexane yield (Table 4, entry 1). This may be due to the competitive adsorption of guaiacol on acid sites of zeolite. As shown in Table 5 (entry 4 and 7), addition of guaiacol reduces the reaction rate of MCH dehydration on zeolite. Fig. 6B shows the adsorption capacities of guaiacol on Hβ with different Si/Al ratios. Obviously, the adsorption amount of guaiacol varies conversely with the Si/Al ratio of Hβ. The large amount of guaiacol adsorbed on Hβ(12.5) definitely inhibits the conversion of MCH on zeolite. Moreover, Hβ with low Si/Al ratio tends to deactivate due to its fast coke formation on excessive acid sites, which was confirmed by TG result of used catalysts (Fig. 7). As shown in Fig. 7, when the temperature is lower than 100 °C, catalyst has little weight loss on the TG curve arising from evaporation of water. During 100–500 °C, there is large weight loss on the TG curve, due to the oxidation of coke on the catalyst. According to quantitative analysis, the ratio of coke deposited on catalysts are 10.14% (Hβ(12.5)), 9.22% (Hβ(20)), 8.32% (Hβ(50)) and 8.29% (Hβ(250)), respectively.

However, Hβ(250) with high Si/Al ratio is also not good choice for guaiacol HDO to cyclohexane. As described in Section 3.5, acid-catalyzed dehydration of MCH on Hβ zeolite is the rate-determining step in this tandem reaction. For Hβ with high Si/Al ratio, insufficient acid sites cannot effectively promote the conversion of MCH, and then result in enhanced yield of MCH. Competitive adsorption of guaiacol and MCH conversion on acid sites of zeolite are conflict with each other, and the key is to balance both in this reaction system. As a compromise, Hβ zeolite with Si/Al molar ratio of 50, possessing moderate acid density, gives the highest yield of cyclohexane in the reaction of guaiacol HDO.
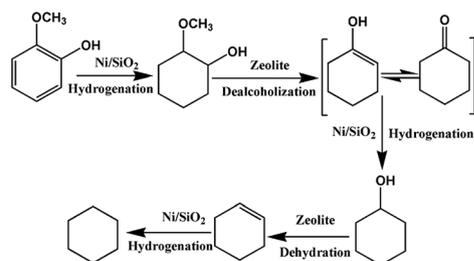
Table 5 Catalytic performance of different catalysts for the conversion of different substrates[a]

Entry	Substrate	Catalyst	Time	Conv. (%)	Main product
1	Guaiacol	Ni/SiO_2	5 h	>99	MCH
2	Guaiacol	Hβ(50)	5 h		Coke
3	MCH	Ni/SiO_2	5 h	—	—
4	MCH	Hβ(50)	10 min	72.9	Cyclohexanone
5	Cyclohexanol	Ni/SiO_2	5 min	—	—
6	Cyclohexanol	Hβ(50)	5 min	90.9	Cyclohexene
7	Guaiacol + MCH	Hβ(50)	10 min	MCH (12%)	Cyclohexanone

[a] Reaction conditions: substrate, 80.6 mmol; catalyst, 50.0 mg; decalin, 20 mL; 140 °C, 3 MPa H_2.

3.5. Reaction pathway of guaiacol HDO over bifunctional catalytic system

Fig. 8A plots the conversion of guaiacol *versus* reaction time at 140 °C over Ni/SiO_2 physically mixed with Hβ(50). The reaction progress was accompanied by a decrease of guaiacol (reactant) and increase of cyclohexane (end-product). MCH and cyclohexanol are the main intermediate products in HDO progress of guaiacol. Further conversion of MCH is the rate-determining step in this cascade reaction. As displayed in Fig. 8B, the guaiacol conversion and MCH yield increased with increasing reaction time from 1 h to 5 h over Ni/SiO_2. However, further conversion of MCH to cyclohexane did not occur even for long reaction time of 5 h. It is obvious that the acid sites of zeolite are the indispensable active sites for deoxygenation. Meanwhile, the addition of zeolite greatly accelerated the conversion of guaiacol and promoted HDO process. The synergistic effect of active metal sites and acid sites are critical to guaiacol HDO reaction.[38,39]

To probe the network of guaiacol conversion in this system, many evaluations were conducted by using different reactants (guaiacol, MCH or cyclohexanol) over selected catalyst (Ni/SiO_2 or Hβ(50)) (Table 5). As shown in Table 5, the initial reactant of guaiacol could be converted into MCH on Ni/SiO_2 with high selectivity, while there was only coke produced only on Hβ(50) (Table 5, entry 1 and 2). Thus, we can infer that guaiacol is first transformed into MCH on Ni/SiO_2. According to entry 3 and 4 in Table 5, the intermediate product MCH was degraded rapidly into cyclohexanone on Hβ(50), and no reaction happened on Ni/SiO_2. Similar to MCH, the dehydration of cyclohexanol into cyclohexene takes place on Hβ rather than Ni/SiO_2 (Table 5, entry 5 and 6). Hβ provides the active sites for conversion of MCH and cyclohexanol. Based on the above experimental

results, the reaction pathway of guaiacol conversion is summarized in Scheme 2. The initial product of MCH from guaiacol hydrogenation on Ni/SiO_2 is converted into cyclohexanone by dealcoholization on zeolite and subsequently hydrogenation to cyclohexanol on Ni/SiO_2. Then, intermediate cyclohexanol is quickly transformed into cyclohexane in dehydration–hydrogenation pathway.

However, olefin species was not typically observed during the whole reaction process of guaiacol conversion on Ni/SiO_2 mixed with Hβ(50). This suggests that the reaction rate of olefin hydrogenation on Ni/SiO_2 is faster than that of alcohols dehydration on Hβ. Compared with guaiacol reaction over only Ni/SiO_2, the fast conversion of MCH on Hβ(50) promotes the degradation rate of guaiacol according to the law of chemical equilibrium. We could further accelerate the reaction rate by modulating the mass of Hβ(50).

Obviously, over Ni/SiO_2 physically mixed with Hβ(50), the high-efficiency transformation of guaiacol to cyclohexane is achieved at very low reaction temperature. As shown in Table 6, guaiacol HDO over representative catalysts carried out at high reaction temperatures, which were higher than 240 °C for non-precious Ni-based catalysts. In contrast, in our catalytic system, the transformation of guaiacol to cyclohexane proceeded at very low temperature of 140 °C, and the maximum yield of cyclohexane was up to 91.7% for 2.5 h. The realization of guaiacol HDO with high cyclohexane yield under low temperature is ascribed to the perfect combination of Ni/SiO_2 with Hβ(50).

On the one hand, guaiacol can be highly selective hydrogenated into MCH on Ni/SiO_2 at low temperature (140 °C).[15] In this work, HDO of guaiacol to cyclohexane mainly proceeded in hydrogenation–dehydration pathway (Scheme 1). However, oxygen removal of guaiacol on previous catalysts was realized by
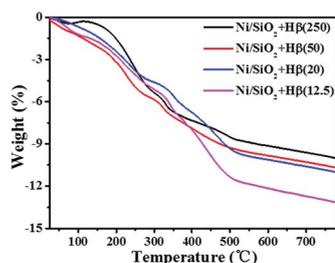

Fig. 7 TG curves of used catalysts containing Ni/SiO_2 and Hβ with different Si/Al ratio.
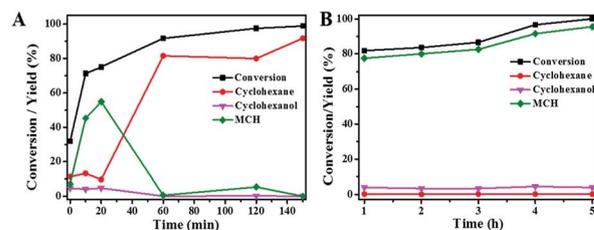

Fig. 8 The product distribution trends of guaiacol HDO with reaction time over (A) Hβ mixed with Ni/SiO_2 and (B) Ni/SiO_2. Reaction conditions: guaiacol (0.10 g), Hβ(50) (50 mg), Ni/SiO_2 (50 mg), decalin (20 mL), 140 °C, 3 MPa H_2.

Table 6 Catalytic behavior of representative catalysts for the transformation of guaiacol to cyclohexane

Entry	Catalyst	T (°C)	P_{H_2} (MPa)	Conv. (%)	Yield^a (%)	Ref.
1	Pt/zeolite	250	4	>90	45.3	9
2	Pt/Al-SBA-15	220	3	100	80	40
3	Pd/C + zeolite	275	1.5	100	0.3	33
4	Pd/C + H_3PO_4	250	5	100	75.7	6
5	Ru/SiO_2–Al_2O_3	250	4	100	60	8
6	Pd/WO_x/γ-Al_2O_3	300	7	100	88	41
7	Pt/H-MFI-90	180	5	100	93	10
8	Nix-Fey/CNT	400	3	96.8	80.7	13
9	Ni/MCM-41 + HZSM5	240	5	100	84.1	42
10	NiMo/SBA-15	250	5	90	56	43
11	Ni/SiO_2–ZrO_2	300	5	100	96.8	12
12	Ni/TiO_2–ZrO_2	300	4	100	86.4	11
13	Sulfided Ni/W/TiO_2	300	7	100	16	44
14	Ni/SiO_2 + Hβ(50)	140	3	>99	91.7	This work

^{a} Yield: yield of cyclohexane.

hydrogenation–deoxygenation in pathway 1 and direct-deoxygenation in pathway 2, simultaneously (Scheme 1). Compared with pathway 1, guaiacol hydrogenolysis to phenolic compounds in pathway 2 needs to cleave C–O bond whose bond energy is higher than that of C=C$_{ring}$. Transformation of guaiacol into cyclohexane in pathway 1 can realize at lower reaction temperature than that in pathway 2.

On the other hand, Hβ(50) is the optimum zeolite for MCH dehydration due to its three-dimensional pore structure with 12-membered ring and suitable acid properties. For large pores of 12-membered ring channels in Hβ, both internal and external acid sites can contribute to the dehydration pathway, realizing high conversion of MCH. Suitable acid properties can effectively balance the competitive adsorption of guaiacol and conversion of MCH on zeolite, and then obtain high yield of cyclohexane.

4. Conclusions

A new and efficient bifunctional catalyst has been developed for guaiacol HDO to cyclohexane at low temperature. By this catalytic system, 2-methoxycyclohexanol (MCH) produced from guaiacol hydrogenation can be easily converted into cyclohexane by multistep reactions of dehydration–hydrogenation on zeolite and Ni/SiO$_2$ in sequence. Typically, guaiacol was successfully converted into cyclohexane with 91.7% yield at 140 °C over Ni/SiO$_2$ combined with Hβ(50). The superior catalytic performance is ascribed to unique pore structure and appropriate acid properties of Hβ(50). Compared with other zeolites (HUSY, HMOR, SAPO34 and HZSM-5), Hβ with three-dimensional large pore structure is benefit for the diffusion of reactant and products. Meanwhile, weak acid property of Hβ reduces the adsorption strength of guaiacol, and thus decreases the toxic effect of guaiacol on acid sites. Moreover, proper acid density of Hβ(50) can effectively balance the competitive adsorption of guaiacol and conversion of alcohols on acid sites, enabling to achieve high yield of cyclohexane. Expectedly, such a low-cost and efficient bifunctional catalytic system will hold potential for the hydrodeoxygenation of bio-oil.

Conflicts of interest

There are no conflicts to declare.

References

1 M. Stocker, *Angew. Chem., Int. Ed.*, 2008, **47**, 9200–9211.
2 D. M. Alonso, J. Q. Bond and J. A. Dumesic, *Green Chem.*, 2010, **12**, 1493–1513.
3 D. Mohan, C. U. Pittman Jr and P. H. Steele, *Energy Fuels*, 2006, **20**, 848–889.
4 E. Furimsky, *Appl. Catal., A*, 2000, **199**, 147–190.
5 P. M. Mortensen, J. D. Grunwaldt, P. A. Jensen, K. G. Knudsen and A. D. Jensen, *Appl. Catal., A*, 2011, **407**, 1–19.
6 C. Zhao, Y. Kou, A. A. Lemonidou, X. Li and J. A. Lercher, *Angew. Chem., Int. Ed.*, 2009, **48**, 3987–3990.
7 D. C. Elliott, *Energy Fuels*, 2007, **21**, 1792–1815.
8 C. R. Lee, J. S. Yoon, Y.-W. Suh, J.-W. Choi, J.-M. Ha, D. J. Suh and Y.-K. Park, *Catal. Commun.*, 2012, **17**, 54–58.
9 E. H. Lee, R. Park, H. Kim, S. H. Park, S.-C. Jung, J.-K. Jeon, S. C. Kim and Y.-K. Park, *J. Ind. Eng. Chem.*, 2016, **37**, 18–21.
10 M. Hellinger, H. W. P. Carvalho, S. Baier, D. Wang, W. Kleist and J. D. Grunwaldt, *Appl. Catal., A*, 2015, **490**, 181–192.
11 X. Zhang, J. Long, W. Kong, Q. Zhang, L. Chen, T. Wang, L. Ma and Y. Li, *Energy Fuels*, 2014, **28**, 2562–2570.
12 X. Zhang, Q. Zhang, L. Chen, Y. Xu, T. Wang and L. Ma, *Chin. J. Catal.*, 2014, **35**, 302–309.

13 H. Fang, J. Zheng, X. Luo, J. Du, A. Roldan, S. Leoni and Y. Yuan, *Appl. Catal., A*, 2017, **529**, 20–31.

14 M. V. Bykova, D. Y. Ermakov, V. V. Kaichev, O. A. Bulavchenko, A. A. Saraev, M. Y. Lebedev and V. A. Yakovlev, *Appl. Catal., B*, 2012, **113**, 296–307.

15 X. Wang, S. Zhu, S. Wang, J. Wang, W. Fan and Y. Lv, *Appl. Catal., A*, 2018, **568**, 231–241.

16 S. Zhu, Y. Zhu, S. Hao, H. Zheng, T. Mo and Y. Li, *Green Chem.*, 2012, **14**, 2607–2616.

17 S. Raju, M.-E. Moret and R. J. M. Klein Gebbink, *ACS Catal.*, 2015, **5**, 281–300.

18 H. Kobayashi, H. Yokoyama, B. Feng and A. Fukuoka, *Green Chem.*, 2015, **17**, 2732–2735.

19 S. Zhu, Y. Xue, J. Guo, Y. Cen, J. Wang and W. Fan, *ACS Catal.*, 2016, **6**, 2035–2042.

20 L. Chen, R.-W. Wang, S. Ding, B.-B. Liu, H. Xia, Z.-T. Zhang and S.-L. Qiu, *Chem. J. Chin. Univ.*, 2010, **31**, 1693–1696.

21 F. F. Madeira, K. Ben Tayeb, L. Pinard, H. Vezin, S. Maury and N. Cadran, *Appl. Catal., A*, 2012, **443**, 171–180.

22 J. Jae, G. A. Tompsett, A. J. Foster, K. D. Hammond, S. M. Auerbach, R. F. Lobo and G. W. Huber, *J. Catal.*, 2011, **279**, 257–268.

23 J. Gu, Z. Zhang, P. Hu, L. Ding, N. Xue, L. Peng, X. Guo, M. Lin and W. Ding, *ACS Catal.*, 2015, **5**, 6893–6901.

24 Y. Liu and Z. Gao, *Acta Pet. Sin., Pet. Process. Sect.*, 1996, **12**, 35–40.

25 J. Bao, J. He, Y. Zhang, Y. Yoneyama and N. Tsubaki, *Angew. Chem.*, 2008, **120**, 359–362.

26 M. D. Foster, I. Rivin, M. M. J. Treacy and O. Delgado Friedrichs, *Microporous Mesoporous Mater.*, 2006, **90**, 32–38.

27 J. Horáček, G. Šťávová, V. Kelbichová and D. Kubička, *Catal. Today*, 2013, **204**, 38–45.

28 A. García-Trenco and A. Martínez, *Appl. Catal., A*, 2012, **411–412**, 170–179.

29 G. Poncelet and M. L. Dubru, *J. Catal.*, 1978, **52**, 321–331.

30 C. A. Emeis, *J. Catal.*, 1993, **141**, 347–354.

31 J. Chang, T. Danuthai, S. Dewiyanti, C. Wang and A. Borgna, *ChemCatChem*, 2013, **5**, 3041–3049.

32 M. Hellinger, S. Baier, P. M. Mortensen, W. Kleist, A. D. Jensen and J.-D. Grunwaldt, *Catalysts*, 2015, **5**, 1152–1166.

33 H. Shafaghat, P. S. Rezaei and W. M. A. W. Daud, *RSC Adv.*, 2015, **5**, 33990–33998.

34 C. D. Baertsch, K. T. Komala, Y.-H. Chua and E. Iglesia, *J. Catal.*, 2002, **205**, 44–57.

35 T. Liang, J. Chen, Z. Qin, J. Li, P. Wang, S. Wang, G. Wang, M. Dong, W. Fan and J. Wang, *ACS Catal.*, 2016, **6**, 7311–7325.

36 H. Knozinger, *Angew. Chem., Int. Ed.*, 1968, **7**, 791–805.

37 W. Song, Y. Liu, E. Barath, L. L. Wang, C. Zhao, D. Mei and J. A. Lercher, *ACS Catal.*, 2016, **6**, 878–889.

38 R. Shu, Y. Xu, L. Ma, Q. Zhang, P. Chen and T. Wang, *Catal. Commun.*, 2017, **91**, 1–5.

39 W. Song, Y. Liu, E. Barath, C. Zhao and J. A. Lercher, *Green Chem.*, 2015, **17**, 1204–1218.

40 M. S. Jang, R.-s. Park, I.-G. Lee, J. M. Kwak, Y.-K. Park and C. H. Ko, *Res. Chem. Intermed.*, 2016, **42**, 3–17.

41 Y.-K. Hong, D.-W. Lee, H.-J. Eom and K.-Y. Lee, *Appl. Catal., B*, 2014, **150**, 438–445.

42 S. Qiu, Y. Xu, Y. Weng, L. Ma and T. Wang, *Catalysts*, 2016, **6**, 134–149.

43 B. M. Q. Phan, Q. L. M. Ha, N. P. Le, P. T. Ngo, T. H. Nguyen, T. T. Dang, L. H. Nguyen, D. A. Nguyen and L. C. Luu, *Catal. Lett.*, 2015, **145**, 662–667.

44 Y.-K. Hong, D.-W. Lee, H.-J. Eom and K.-Y. Lee, *J. Mol. Catal. A: Chem.*, 2014, **392**, 241–246.